ON THE USE OF THE RADON TRANSFORM IN STUDYING NEARSHORE WAVE DYNAMICS

Rafael Almar[1], Philippe Bonneton[2], Hervé Michallet[3], Rodrigo Cienfuegos[4], Gerben Ruessink[5] and Marion Tissier[5]

Abstract

In nearshore studies, there is an increasing interest for describing wave-by-wave dynamics. Most existing methods compute bulk parameters for celerity and the separation of incoming and outgoing waves. In this paper we address the use of the Radon Transform for studying wave dynamics. The Radon Transform is a projection of a bidimensional field (e.g. spatiotemporal wave signal) into polar coordinates which can be back projected at given angles. The method is applied to laboratory low-sloping beach and non-linear waves GLOBEX dataset. The separation of incoming from outgoing long waves using Radon is tested and compared to the method described in Guza et al., (1984). Components are retrieved, even at standing long wave nodes. Individual short wave celerity derived from Radon is found in agreement with celerity derived from tracked individual crest.

Key words: Radon transform, Separation of incoming and outgoing waves, nearshore, individual celerity, infragravity waves, beach reflection, laboratory experiment

1. Introduction

The complexity of an incident short-wave (typically, 0.05-0.5 Hz) field increases while approaching the shore. For example, short waves induce long waves (~0.005-0.05 Hz) that reflect from the beach face, producing cross-shore patterns that may influence individual short waves (Roelvink and Stive, 1989; Abdelrahman and Thornton, 1987). Limitations regarding the available incoming and outgoing signal separation techniques presently prevent an accurate description and understanding of wave-by-wave dynamics and wave-to-wave interactions between incident and outgoing wave fields. The celerity of short waves, for example, can be estimated through cross-correlation techniques (Tissier et al., 2011), which become very inaccurate when applied to individual waves. As pointed out by Baldock et al. (2006), no rigorous separation procedure exists for irregular waves breaking over a sloping bed. Signal separation often relies on spectral approaches based on Fourier transformed wave time-series on a subarray of adjacent wave gauges (e.g. Goda and Suzuki, 1974; Sheremet et al., 2002; Battjes et al., 2004; van Dongeren et al., 2007). Moving toward methods that estimate the amplitudes and phases of incident and reflected waves is required to perform wave-by-waves analysis, opening up new research possibilities.

In this work, we aim to assess the ability of the Radon transform (RT, Radon, 1917; Deans, 1983) in

[1]IRD-LEGOS (CNES/CNRS/IRD/University of Toulouse), Avenue Edouard Belin, 31400 Toulouse, France. rafael.almar@ird.fr

[2]UMR EPOC, University of Bordeaux, Avenue des Facultés, Talence 33405, France. p.bonneton@epoc.u-bordeaux1.fr

[3]CNRS/UJF/G-INP, UMR LEGI, BP53, 38041, Grenoble, France, herve.michallet@legi.grenoble-inp.fr

[4]DIHA, Pontificia Universidad Catolica de Chile, Vicuña Mackenna 4860, Macul, Santiago, Chile, racienfu@ing.puc.cl

[5]Department of Physical Geography, Faculty of Geosciences, Utrecht University, P.O. Box 80.115, 3508 TC Utrecht, The Netherlands, m.f.s.tissier@uu.nl; b.g.ruessink@uu.nl

describing nearshore wave dynamics from dense spatiotemporal data of sea surface elevation. The RT has been commonly used in image processing and computer vision as edge detector, de-noising, and line extraction (Murphay, 1986). In geosciences, applications exist in the field of seismology (de Hoop et al., 2008), ship waves (Rey et al., 1990), regional ocean Rossby waves propagation (Cipollini et al., 1998). Nearshore use includes the tracking of the crests of individual waves (Yoo et al., 2008) and in the detection of the swash front motion (Zhang et al., 2009).

Here, we address the use of the RT in the context of describing nearshore wave dynamics. The RT is applied to the EU-Hydralab IV GLOBEX laboratory experiment (non-linear conditions, see Ruessink et al., 2013). The performances of the RT are compared with traditional methods. We show that it is a powerful tool to separate incoming and outgoing waves and to estimate the celerity of individual short waves. We also discuss the advantages, limitations and perspectives of the method for coastal studies.

2. The Radon Transform

The RT (Radon, 1917; Deans, 1983; Duda and Hart, 1972) $R(\rho,\theta)$ is an angular projection of a two-dimension field $\eta(x,t)$ over a line as defined by:

$$R(\rho,\theta) = \iint \eta(x,t)\delta(x\cos\theta + t\sin\theta - \rho)\mathrm{d}x\mathrm{d}t \qquad (1)$$

Here, θ (ranging from 0° to 180°) and ρ are the angle and radius that define the line, in polar coordinates, on which the function is projected, x and y are orthonormal coordinates, δ is the Dirac delta function. The use of the Dirac delta function forces the integration of $\eta(x,t)$ along the line defined by $\rho = x\cos\theta + t\sin\theta$.

If a two-dimensional spatiotemporal wave signal, $\eta(x,t)$, is considered, the resulting θ can be converted into a wave celerity C through the following transformation:

$$C = \tan(\theta)dx/dt \qquad (2)$$

where dx and dt are the spatial and temporal resolution, respectively.

In Figure 1 is illustrated the principle of the estimation of wave-by-wave celerity using the RT. If the $\eta(x,t)$ signal contains multiple waves, multiple local peaks (ρ,θ) will be identified by the application of the RT. Propagating crests in the spatiotemporal $\eta(x,t)$ field (Figure 1.a) are detected from their signature in the Radon space (Figure 1.b), corresponding to peak values. The θ-coordinate of the peak gives the crest propagation angle. This angle is further converted into celerity using Equation 2. Interestingly, wave trough celerity can also be determined from its signature corresponding to a minimum in the Radon space. This can be useful for intra phase wave description, when asymmetry increase.

In the case of a spatiotemporal wave field containing incoming and outgoing waves, $\eta(x,t) = \eta_{In}(x,t) + \eta_{Out}(x,t)$, each component can be retrieved using the inverse RT. The inverse RT is a back-projection of $R(\rho,\theta)$ at given angles θ. The total initial wave signal $\eta(x,t)$ can be reconstructed as:

$$\eta(x,y) = \iint R(\rho,\theta)\mathrm{d}\theta\mathrm{d}\rho \qquad (3)$$

$\eta_{In}(x,t)$ and $\eta_{Out}(x,t)$ can also be separated from waves propagation angle:

$$\eta_{In}(x,t) = \int_{-\infty}^{+\infty}\int_{1}^{89} R(\rho,\theta)\mathrm{d}\theta\mathrm{d}\rho \qquad (4)$$

$$\eta_{Out}(x,t) = \int_{-\infty}^{+\infty}\int_{91}^{179} R(\rho,\theta)\mathrm{d}\theta\mathrm{d}\rho \qquad (5)$$
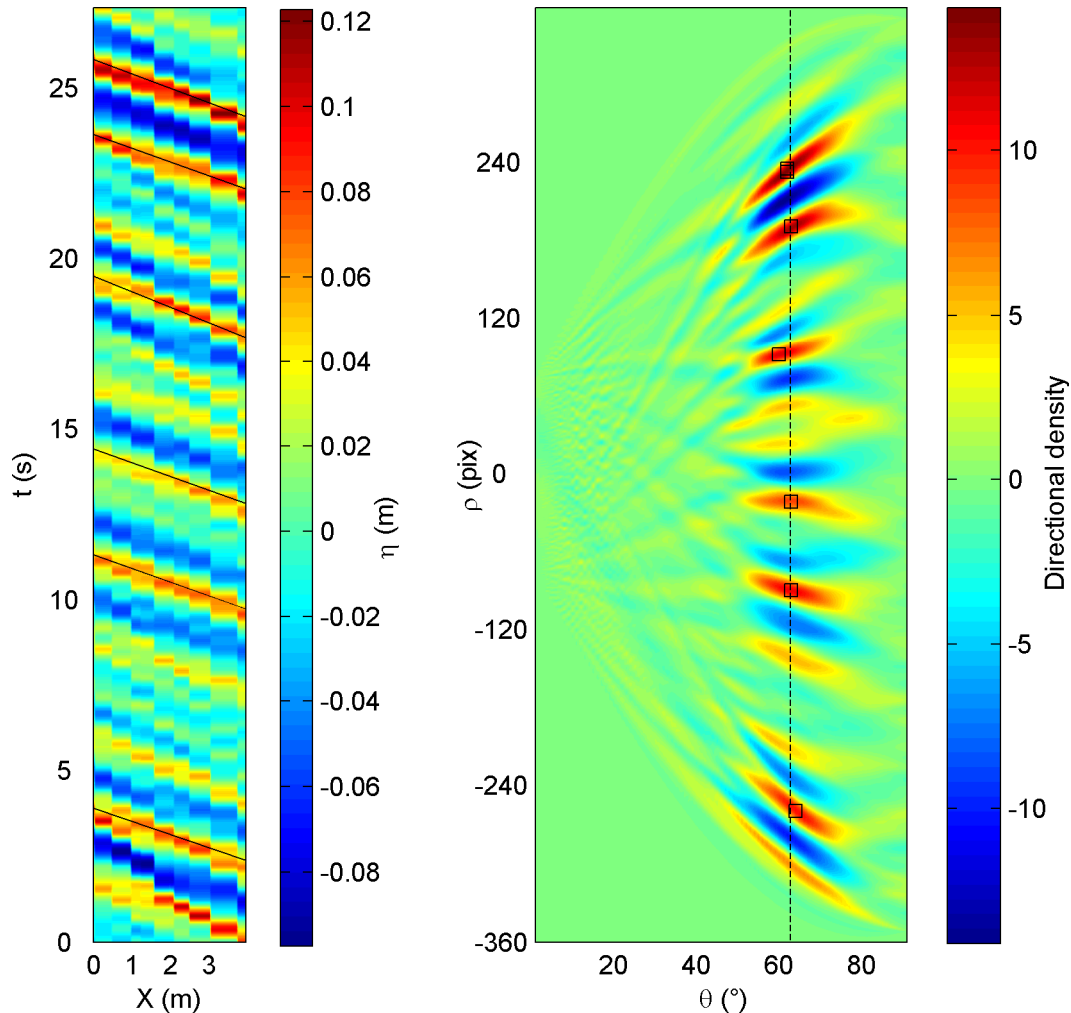
Figure 1. Illustration of the use of Radon Transform for wave-by-wave celerity estimation. a) Spatiotemporal field of short-wave surface elevation and b) its Radon Transform expressed as a directional density (or distribution). In a) crest trajectories (black lines) are shown and corresponding local maxima (black squares) locations give crests propagation angle. In b) the dashed line represents the mean detected crests angle.

3. GLOBEX laboratory experiment

A laboratory experiment was undertaken in the Deltares 110 m wave flume (Scheldegoot) within the framework of the EU-Hydralab IV project (Ruessink et al., 2013). One of the goals was to study non-linear wave transformation and the interactions between short and long waves. Eight wave conditions were considered during this experiment (3 random, 3 bichromatic and 2 monochromatic cases), and were repeated 10 times for different instrument positions. This results in a total of 190 measurement locations for the free-surface elevation and 43 for the velocity per wave condition, recorded with a sampling frequency F_s=128 Hz. For the purpose of this study, random waves A2 series (JONSWAP with peak enhancement factor of $\gamma = 3.3$, significant wave height H_s=0.2 m and peak frequency f_p=0.44 Hz) and bichromatic waves B2 series (primary frequencies of f_1=0.42 Hz and f_2=0.462 Hz

with associated amplitudes of A_1=0.09 m and A_2=0.01 m, respectively) were used. Further details concerning the experimental set-up and data pre-processing can be found in Ruessink et al. (2013).

4. Applications of the Radon Transform to coastal waves' dynamics

4.1 Separation of incoming and outgoing waves
In this section, the RT method is compared to the commonly used Guza et al. (1984) method (hereafter referred as Guza84). In Guza84, shoreward and seaward propagating long waves (η_+ and η_-, respectively) are constructed from collocated surface elevation η and cross-shore velocity u timeseries using the assumptions of shallow water and cross-shore propagation:

$$\eta_\pm = 0.5 \, [\eta \pm u \, . \, (h/g) \, {}^\wedge 0.5] \tag{6}$$

where h is the water depth and g gravitational acceleration.
For the use of this method, both current and elevation signals are low pass filtered (fc=3/5fp) to keep only long waves.

Figure 2 shows the spatiotemporal evolution of original surface elevation signal and the RT estimated incoming and outgoing components for the random A2 (left panels) and bichromatic B2 (right panels) cases. For A2, it can be seen in Figure 2.a that short-wave convergence and divergence is strong, due to the presence of a large underlying long-wave signal. The incoming short- and long-wave patterns (Figure 2.c) were recovered as well as the outgoing reflected long waves (Figure 2.e). Outgoing long waves were much lower frequency than the incident ones. This can be clearly seen in the low frequency surface elevation timeseries in Figure 3.a which describes the propagation and deformation of incoming and outgoing waves. The observed contrast between incoming and outgoing patterns is believed to facilitate the performances of separation methods. The energy conservation of the RT method was tested by comparing original long wave amplitude with the combination of the RT estimation of incoming and outgoing components (Figure 4.a). A good agreement was found between reconstructed and original amplitudes with a mean quadratic difference of 2 %. The RT performance was tested against Guza84 in the Figure 4.b which shows the amplitude of incident and reflected waves, estimated from the two methods. Results indicate that the methods are in good agreement. The energy reflection of long waves computed from RT is in the order of 5 %. See De Bakker et al. (2013) for additional analyses.

The bichromatic waves B2 case is characterized by regular incident wave groups (f=0.462-0.42=0.042 Hz, Figure 2.b) and hence monochromatic long-waves that, at least, partly reflected from the beach and propagate offshore (Figure 3.b). Consequently, a strong standing pattern is present. Contrary to what was observed for A2, the period of the incoming and outgoing long waves is similar, representing challenging conditions for the separation methods, particularly at the nodes. Results shown in Figure 2.f indicate that the RT caught outgoing waves throughout the profile. The long-wave standing pattern is visible in both the original and reconstructed amplitudes (Figure 4.c). It is interesting to note, in Figure 3.b (timeseries at the second most offshore location), that the RT was able to identify incident and outgoing wave components even at node locations, where resulting amplitude is close to zero. The RT reconstruction error was found larger than for A2 (quadratic error 6 %), due to this standing pattern (Figure 3.b and Figure 4.c). The incoming and outgoing estimated amplitudes (Figure 4.b) obtained from RT and Guza84 present some discrepancies. Interestingly, Guza84 shows an unexpected large noise around the short-wave's breakpoint (X= 60 m). This should be further investigated but may result from cross-modes in the flume at this location. The energy reflexion of long waves computed from RT is larger than in case A2, around 23 %.

In Figure 3.b, noisy RT surface elevation can be seen at the edge of the bidimensional field. This is inherent to the RT method which has not enough information to accurately compute the propagation angle at the edges. Typically, from geometrical considerations, one can consider that points closer than a characteristic wavelength L=C.T in space and period T=L/C in time from the edges are not reliable (more details provided from synthetic test cases in Almar et al., 2013).
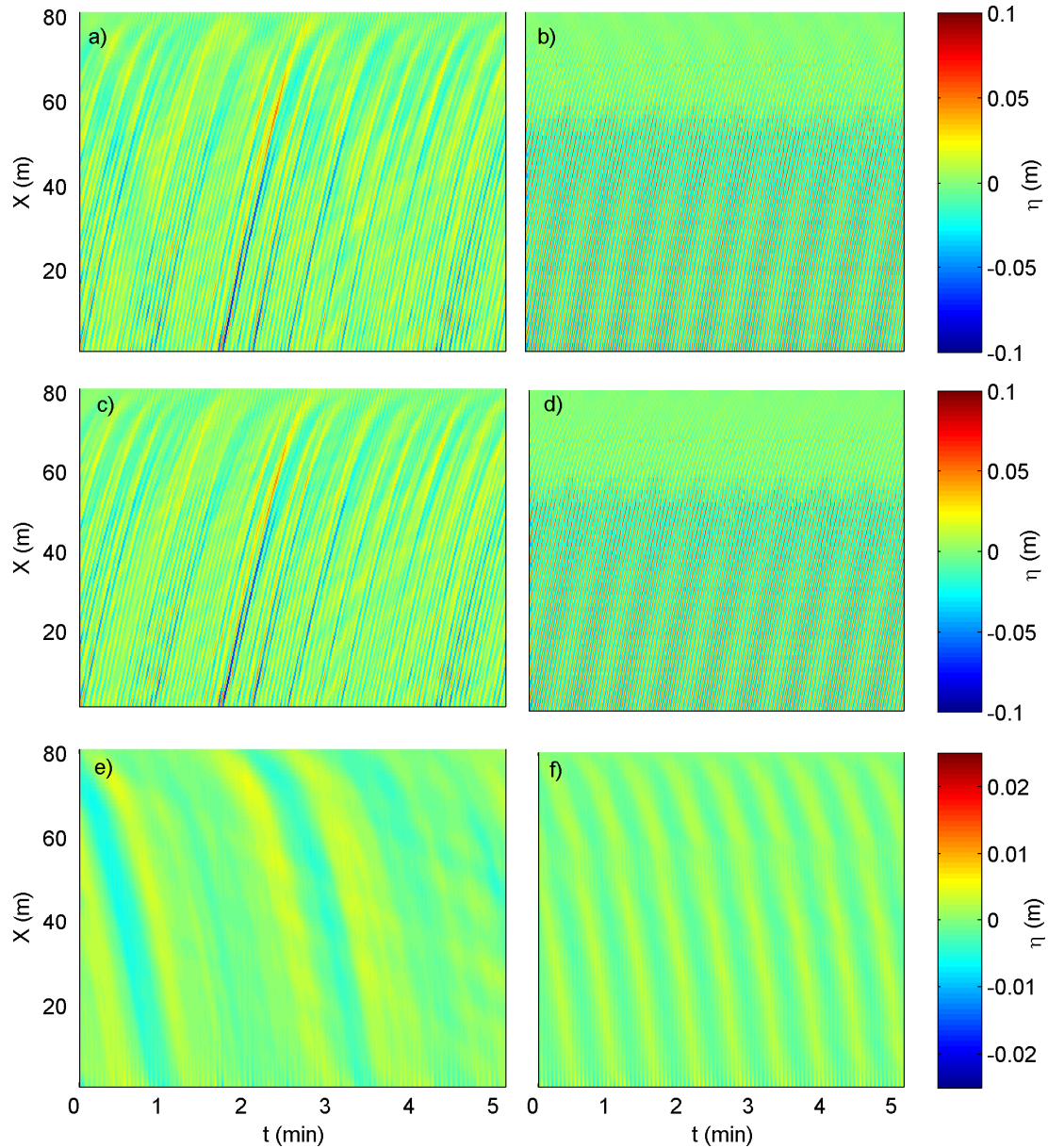

Figure 2. Surface elevation η spatiotemporal evolution along the cross-shore direction X (m). a) Total A2, b) total B2, c) incoming A2, d) incoming B2, e) outgoing A2 and f) outgoing B2 waves fields.
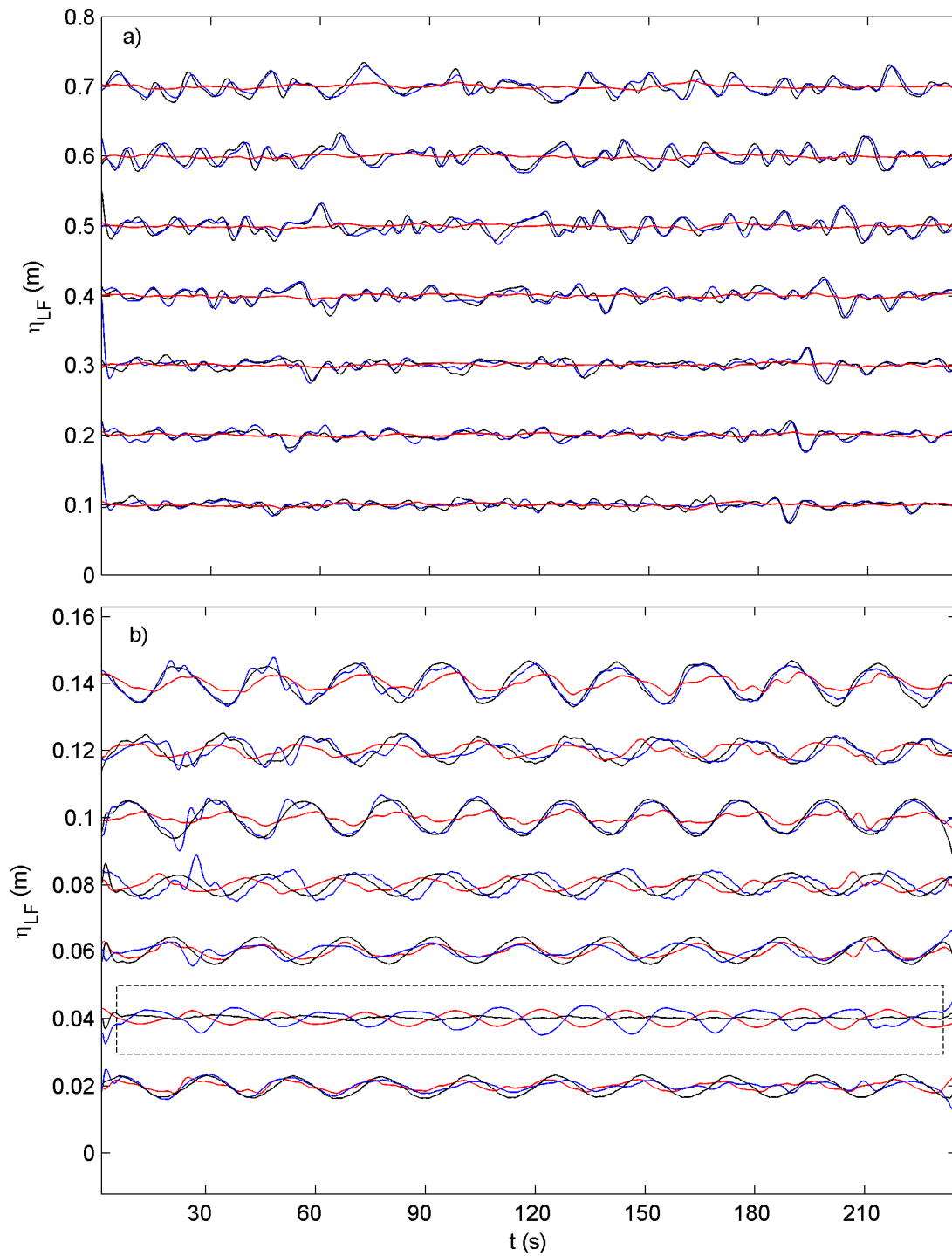
Figure 3. Low frequency (*f*< 3/5 *fp*) surface elevation η_{LF} (m) timeseries every 10 m from the most offshore sensors to the beach (bottom to top) for the a) random A2 and b) bichromatic B2 cases: (black) total, (blue) incoming and (red) outgoing components. Dashed rectangle indicates the location of standing long wave node.
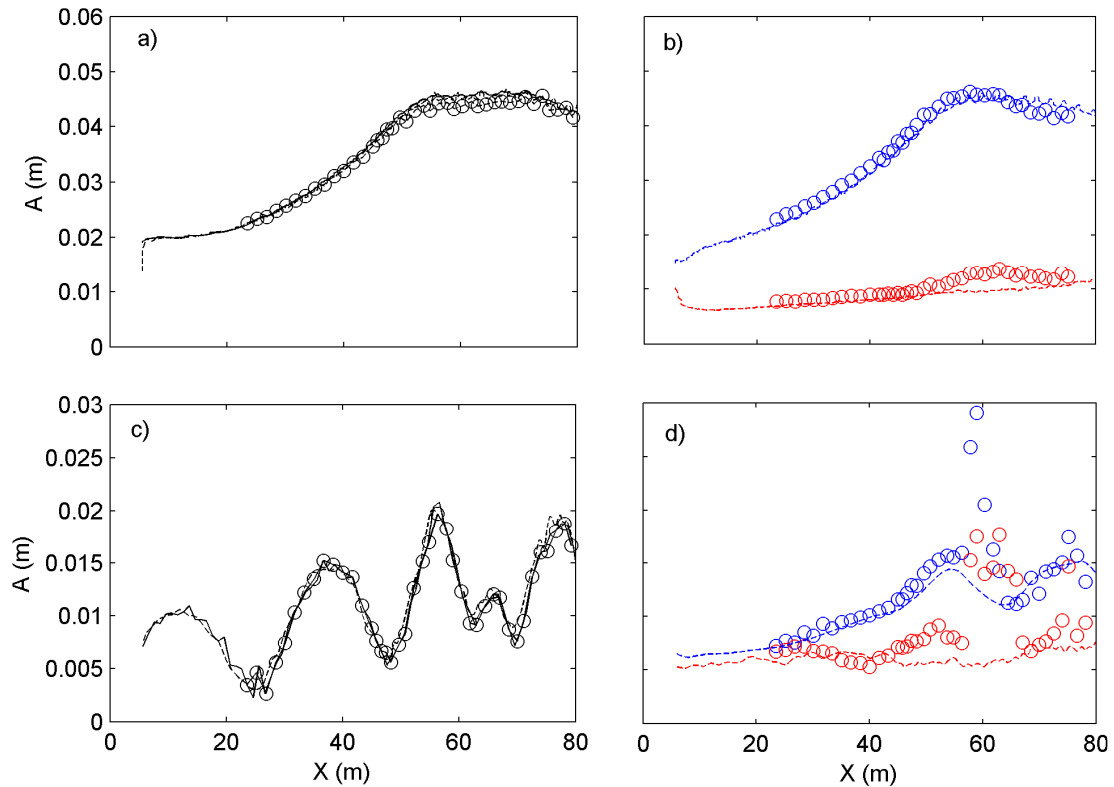
Figure 4. Long-wave amplitude *A* (m) along *X* (m). Total long-wave amplitude (solid line), reconstructed from RT (dashed line) and from Guza84 (circles) for a) A2 and c) B2. Incoming and outgoing waves amplitude, for b) A2 and d) B2, estimated from Guza et al. (1984) (circles) and from Radon (dashed line). Red is outgoing component and blue is ongoing.

4.2 Wave-by-wave celerity estimation

The ability of the RT in estimating wave-by-wave celerity was also tested using GLOBEX data. To compare with the RT estimation, celerities were first derived from automated crest detection on spatiotemporal surface elevation data (Figure 5). At the location of the most offshore sensor, wave crests were detected from local maxima. Individual crest propagation was given by the detection of the crest at neighbor onshore locations. This was done iteratively along the cross-shore sensors array. Spurious points were rejected using the following two criteria: within two consecutive sensors, the crest height variation should not exceed 10% and celerity couldn't be lower than 0.5 m/s. These two conditions allowed rejecting artificial jumps in celerity when the method picked another wave crest. The detection performed better for the bichromatic B2 case than for the random A2 because of numerous waves merging/splitting in the latter. Figure 5 well illustrates the issues encountered when trying to track individual waves crest. For the two cases, approximately 1200 wave trajectories were taken for further consideration. Figure 6 shows the individual celerities as a function of still water depth *D* along the profile, for A2 and B2. Wave-by-wave dispersion was found much larger for A2 (Figure 6.a) than B2 (Figure 6.b). Interestingly, a local maximum of celerity was present for B2 around *D* =-0.3 m which represents the inception of breaking. This is supposed to be associated to the rapid increase of wave asymmetry (see Ruessink et al., 2013 and Tissier et al., 2013 for more GLOBEX analyses) with crests that propagate faster than troughs.
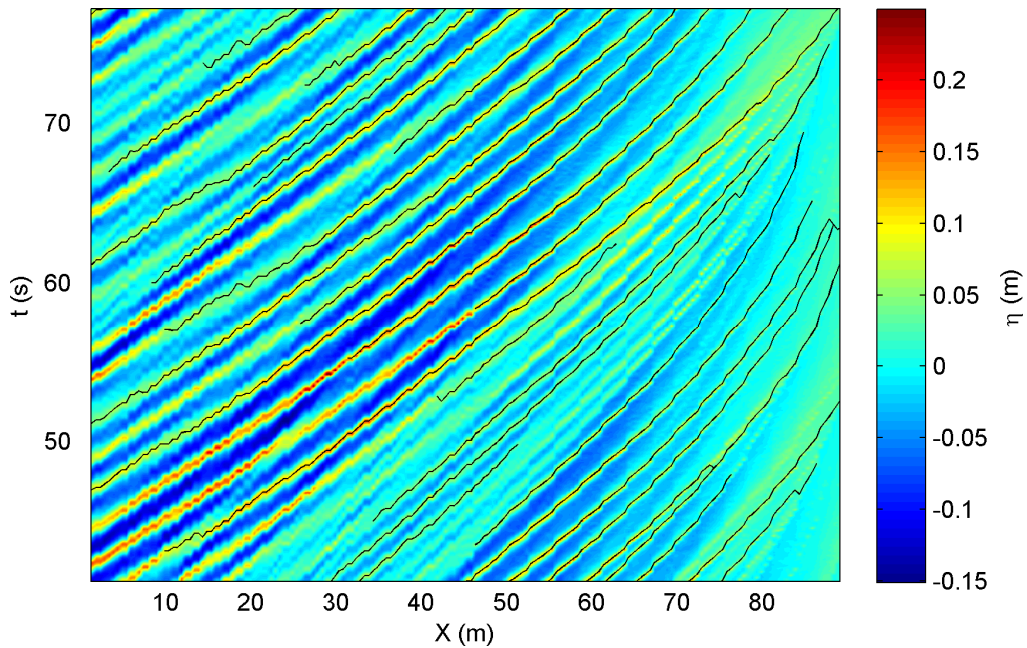
Figure 5. Illustration of the crest tracking method: unfiltered spatiotemporal surface elevation along the cross-shore direction X (m) for the random A2 case. Superimposed black lines stand for the detected crests that passed the quality control.
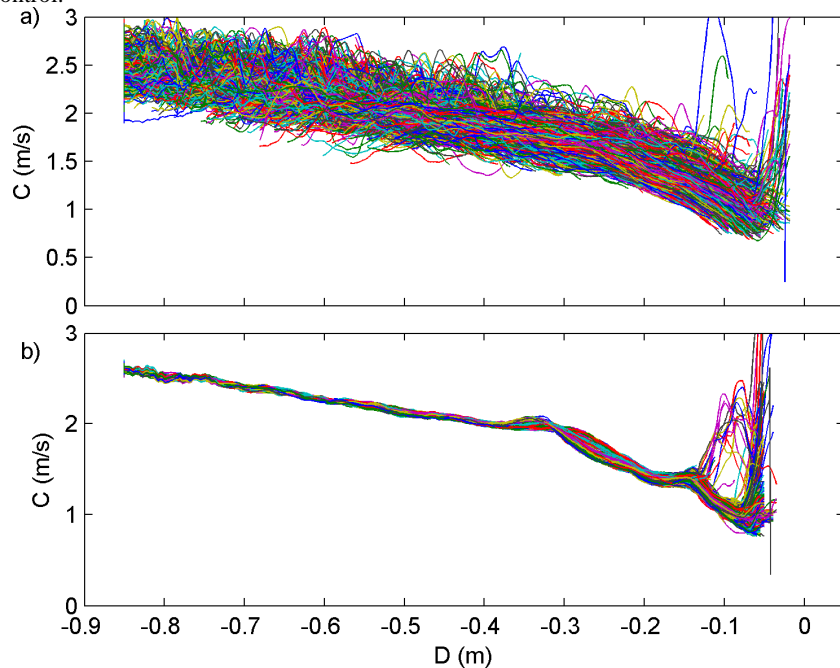

Figure 6. Individual wave (~1000) celerites C estimated from the trajectory tracking method as function of depth D (m) for the a) A2 and b) B2 series.

The wave-by-wave celerity was also estimated from the RT. The spatiotemporal surface elevation signal was first high-pass filtered to conserve only short-wave dynamics. Celerity was estimated within a moving Wx-wide window (here we chose Wx=4 m, about one wavelength) and assumed

constant within *Wx*. The celerities derived from RT were then compared to the ones computed from trajectories. Figure 7 shows computed bulk celerity parameters, average and dispersion (i.e. standard deviation). Along the profile, the quadratic relative difference of average values between methods was 6 % (absolute 0.05 m/s) and 4 % (absolute 0.03 m/s), for A2 and B2 respectively. We hypothesize this difference partially comes from the fact that the two methods do not exactly pick the same waves for the analysis. Quadratic relative difference of dispersion values was 21 % (absolute 0.03 m/s) and 45 % (absolute 0.01 m/s), for A2 and B2 respectively. Of note, the RT caught the behavior observed in Figure 6 with a wave-by-wave celerity dispersion larger for A2 than for B2. See Tissier et al. (2013) for further analyses on GLOBEX wave-by-wave celerity and comparison with estimators.
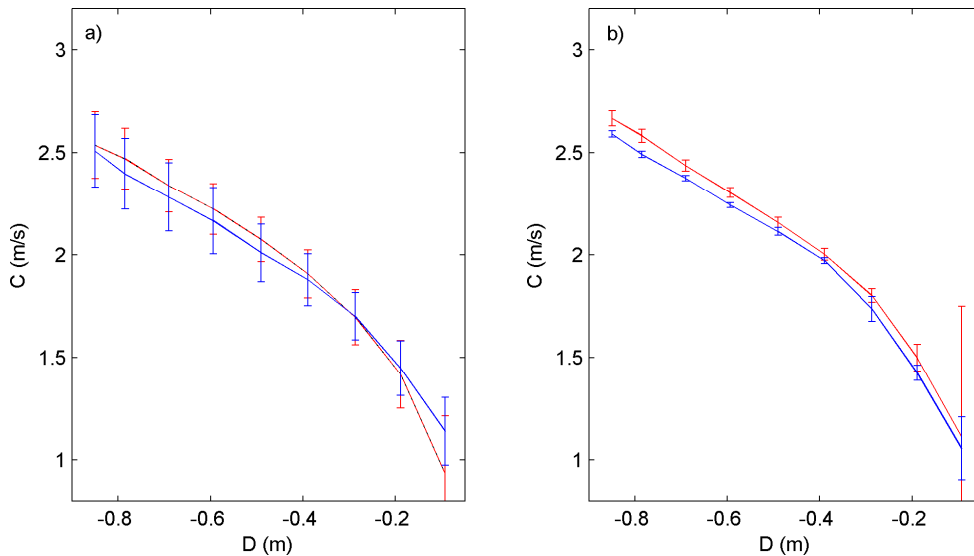

Figure 1. Average celerity derived from wave-by-wave estimation for a) A2 and b) B2. Errorbars stand for dispersion. Red line is RT-derived, blue line trajectory tracked.

3. Concluding remarks

In this paper the Radon Transform (RT) method was tested for studying nearshore wave dynamics. The RT is a transformation of a bidimensional field into a polar space which can be backprojected at given ranges of angle. The method was applied to the GLOBEX laboratory dataset, characterized by 1:80 sloping beach and highly non linear waves. Random and bichromatic wave series were considered. Separation of incoming and outgoing waves is based on the identification, in the polar space, of signal propagating at angles from 1 to 90° (incoming) and 91 to 180° (outgoing). Results showed that the method was able to separate signals. Quadratic error on the total signal reconstruction was lower than 5 % and mainly localized at the edges of the bidimensional field. The standing long wave pattern of the bichromatic case represented challenging conditions for the RT. Long wave energy reflection at the beach was found to be around 5% and 23% for the random and bichromatic case, respectively. The RT was applied to wave-by-wave celerity estimation. This is based on the identification of individual crests signatures in the polar space. Obtained angles are further converted into celerities. The RT showed good skills at retrieving wave-by-wave celerity with quadratic differences lower than 6 % while compared to celerities derived from automated tracked trajectories. The RT approach has the strong advantage of conserving intra-phase characteristics when separating incident and outgoing components. It also brings this new possibility of computing wave-by-wave celerity instead of only a bulk, wave-averaged value. From its new skills, this method should bring new insight on nearshore wave dynamics and particularly in studying the interactions between short and long waves.

References
Abdelrahman, S. M. and Thornton, E. B., 1987. Changes in the short wave amplitude and wavenumber due to the presence of infragravity waves. Proceedings of the Speciality Conference on Coastal Hydraulics, American Society of Civil Engineers, New York, 458-478.
Almar, R, Michallet, H., Cienfuegos, R., Bonneton, P., Tissier, M., Ruessink, G., 2013. On the use of the Radon transform in studying wave dynamics. Coastal Engineering, In Preparation
Almar R., Bonneton P., Senechal N., Roelvink D. 2008. Waves celerity from video imaging: a new method, Proceedings of International Conference on Coastal Engineering, 1(5), 661-673
Baldock, T.E. 2006. Long wave generation by the shoaling and breaking of transient wave groups on a beach. Pro ceedings of the Royal Society of London Series A, 462, 1853-1876
Cipollini, P., Cromwell, D., Quartly, G.D. 1998. Observations of Rossby waves propagation in the Northeast Atlantic with TOPEX/POSEIDON altimetry, Advances in Space Research, 22(11), 1553-1556
De Bakker, A., Tissier, M., Marieu, V., Sénéchal, N., Ruju, A., Lara, J.L. and Ruessink, B.G., 2013. Infragravity w ave propagation and dissipation on a low-sloping laboratory beach, Proceeding of Coastal Dynamics 2013, June 2 013, Arcachon, France
De Hoop, M., Smith, H., Uhlmann, G., Van der Hilst, R. 2008. Seismic imaging with the generalized Radon transform: A curvelet transform perspective, Inv. Probl., 25, 025005
Deans, S., 1983. The Radon Transform and Some of Its Applications, 1st Edition. Wiley, New York
Duda, R. O. and P. E. Hart. 1972. Use of the Hough Transformation to Detect Lines and Curves in Pictures, Comm. ACM, Vol. 15, pp. 11-15
Goda, Y., Suzuki, Y., 1976. Estimation of incident and reflected waves in random wave experiments. In: Proceedings of 15th International Conference on Coastal Engineering. ASCE, Honolulu, HI, pp. 828–845
Guza, R.T., Thorton, E.B., Holman, R.A. 1984. Swash on steep and shallow beaches. Proceedings of the 19th International Conference on Coastal Engineering, ASCE, 708-723
Murphy, L. M. 1986. Linear feature detection and enhancement in noisy images via the radon transform, Patte rn Recognition Letters, vol. 4.
Rey, M. T., Tunaley, J. K., Folinsbee, J. T., Jahans, P. A., Dixon, J. A., Vant, M. R. 1990. Application of Radon transform techniques to wake detection in Seasat-A SAR images, IEEE Trans. Geosci. Remote Sensing, 28, 553 - 560
Roelvink, J. A. and Stive, M. J. F., 1989. Bar-generating cross-shore flow mechanisms on a beach. Journal of Geophysical Research, 94: 4785-4800.
Ruessink, B.G., Michallet, H., Bonneton, P., Mouazé, D., Lara, J.L, Silva, P.A. and Wellens, P., 2013. GLOBEX: Wave dynamics on a gently sloping laboratory beach, Proceeding of Coastal Dynamics 2013, June 2013, Arcacho n, France
Ruju, A. Lara, J.L., Losada, I.J. 2012. Radiation stress and low-frequency energy balance within the surf zone: A numerical approach, Coastal Engineering, 68, 44-55
Sheremet, A., R.T. Guza, S.Elgar, andT. H. C. Herbers. 2002. Observations of nearshore infragravity waves: Seaward and shoreward propagating components, J. Geophys. Res., 107(C8), 3095, doi:10.1029/2001JC000970
Tissier M., Bonneton P., Almar R., Castelle B., Bonneton N., Nahon A. 2011. Field measurements and non-linear prediction of waves celerity in the surf zone, European Journal of Mechanics - B/Fluids, 30, 635-641
Tissier, M. Almar, R., Bonneton, P. Michallet, H., de Bakker, A., Ruessink, B.G., 2013. Role of Short and Long-W ave interaction on wave celerity in the Surf zone of a low-sloping beach, Proceeding of Coastal Dynamics 2013, J une 2013, Arcachon, France
van Dongeren, A.R., Battjes, J.A., Janssen, T.T., van Noorloos, J., Steenbergen, K., Reniers, A. 2007. Shoaling an d shoreline dissipation of low-frequency waves, Journal of Geophysical Research, 112 (C02011)
Yoo, J., 2011. Depth inversion in the surf zone with inclusion of waves non-linearity using video-derived celerity. J. Waterw. Port Coastal Oc. Eng.137 (9)
Zhang, S., Zhang, C., Qi, Z., 2009. Waves swash velocity estimation using ridgelet transform. In: 9th Int. Conf. Electronic Meas. & Instr. ICEMI 09. 1078-1081